Wang et al. *NPG Asia Materials* (2019)11:44
https://doi.org/10.1038/s41427-019-0144-8

NPG Asia Materials

ARTICLE Open Access

Spontaneous cationic ordering in chemical-solution-grown La_2CoMnO_6 double perovskite thin films

Hailin Wang[1], Jaume Gazquez[1], Carlos Frontera[1], Matthew F. Chisholm[2], Alberto Pomar[1], Benjamin Martinez[1] and Narcis Mestres[1]

Abstract

Double perovskite oxides are of interest because of their electric, magnetic, and elastic properties; however, these properties are strongly dependent on the ordered arrangement of cations in the double perovskite structure. Therefore, many efforts have been made to improve the level of cationic ordering to obtain optimal properties while suppressing antisite defect formation. Here, epitaxial double perovskite La_2CoMnO_6 thin films were grown on top of (001)-STO oriented substrates by a polymer-assisted deposition chemical solution approach. Confirmation of the achievement of full Co/Mn cationic ordering was found by scanning transmission electron microscopy (STEM) measurements; EELS maps indicated the ordered occupancy of B–B′ sites by Co/Mn cations. As a result, optimal magnetic properties ($Msat \approx 6\ \mu_B$/f.u. and $Tc \approx 230$ K) are obtained. We show that the slow growth rates that occur close to thermodynamic equilibrium conditions in chemical solution methods represent an advantageous alternative to physical deposition methods for the preparation of oxide thin films in which complex cationic ordering is involved.

Introduction

Complex oxides are a class of materials with a plethora of physical properties of strong interest for many different technological applications from catalysis to spintronics[1,2]. In addition, there are many possibilities to tune their final physical properties by changing their microstructure (structural strain, microstructural defects, and vacancies) and doping rate. On the other hand, the spectacular advance of thin film preparation and characterization techniques has opened the possibility of engineering physical properties of oxides on the atomic scale, which allows the design of devices with new functionalities[3,4].

In this context, transition metal oxides with a double perovskite structure have attracted considerable attention because of their unique electrical, magnetic, and elastic properties[5–7]. The simple ABO_3 chemical formula of perovskites allows for high structural and compositional flexibility, as both A and B sites can accommodate a wide variety of atomic combinations. As a result, in double perovskite $(AA')(BB')O_3$ compounds, in which the A and B sites contain more than one element, cation ordering can play an important role in determining the material properties. In particular, $A_2BB'O_6$ double perovskite physical properties are strongly affected by the cationic ordering of B and B′-site sublattices, which in turn is very sensitive to the particular synthesis conditions. La_2CoMnO_6 (LCMO) exemplifies the challenges associated with structure-property engineering of multicomponent oxide systems[8–11]. When full cationic ordering is achieved, LCMO is a ferromagnetic (FM) semiconductor with a relatively high FM Curie temperature, $T_C \approx 230$ K, making it very attractive for thermoelectric and spintronic applications[12,13]. FM ordering is explained by the superexchange interaction between Mn^{4+} and Co^{2+} according to the Goodenough–Kanamori

Correspondence: Narcis Mestres (narcis.mestres@icmab.es)
[1]Institut de Ciència de Materials de Barcelona (ICMAB), Consejo Superior de Investigaciones Científicas (CSIC), Campus UAB, 08193 Bellaterra, Spain
[2]Materials Science and Technology Division, Oak Ridge National Laboratory, Oak Ridge, TN 37831, USA

rules[14–16], and it is very sensitive to the cationic ordering in the B-sublattice[17]. Spontaneous cationic ordering of the B, B′-site sublattice is difficult to attain, and tedious annealing processes under a controlled atmosphere are usually required. Currently, there is no clear agreement in the literature regarding the most convenient strategy to achieve full cationic ordering, and the benefits and drawbacks of crystal growth close to/far from thermodynamic equilibrium conditions have been discussed[18].

Films prepared by chemical solution deposition methods have the final amount of material with the required stoichiometry already deposited on the substrate at the very beginning of the growth process (ex situ growth process). Therefore, it is expected that the film growth will proceed close to thermodynamic equilibrium conditions, which should promote the high crystallinity and quality of the films[19]. In contrast, physical deposition methods such as pulsed laser deposition (PLD) or radio-frequency (RF) magnetron sputtering deposition are nonequilibrium growth techniques owing to the continuous deposition of material and to the high electronic excitation, degree of ionization, and kinetic energies of the flux of atomic species incident on the substrate[18].

Specifically, in the case of LCMO, most of the results reported in the literature correspond to epitaxial thin films grown by PLD. As mentioned above, crystal growth occurs under conditions far from equilibrium, and ordered occupancy of the B and B′ positions is difficult to attain. Usually, as-grown LCMO films prepared by PLD do not exhibit high cationic ordering, making additional annealing processes in ambient oxygen necessary[10,20,21]. Strategies based on structural strain effects leading to the formation of two different sized B-site spaces in a rock salt arrangement have been recently proposed as a way to induce spontaneous cationic ordering of the B, B′-site sublattice in epitaxial thin films;[22] however, the results are not conclusive. High-quality LCMO thin films have also been prepared by using RF magnetron sputtering. A very narrow window for the growth of the ordered phase was identified; however, an annealing process at sufficiently high temperatures (~900 °C) in an oxygen-rich atmosphere ($P_{O2} > 400$ Torr) is necessary to obtain optimal magnetic properties, which are indicative of a high cationic ordering[23].

Therefore, the precise physicochemical mechanisms that promote spontaneous B-site cationic ordering are still unknown. In this regard, control of the growth kinetics has been proposed as an effective tool to achieve spontaneous cationic ordering because B-site differences may be enhanced at the growth front[24]. For this reason, the use of chemical methods that allow thin film growth close to equilibrium conditions, in contrast to physical growth methods (PLD and sputtering), might be an interesting alternative for obtaining spontaneous cationic ordering. In fact, the growth of LCMO on (111)-$SrTiO_3$ (STO) substrates has been explored using metal–organic aerosol deposition (MAD)[25], and excellent saturation magnetization (*Msat*) and Curie temperature values indicative of high cationic ordering have been obtained.

Polymer-assisted deposition (PAD) is an affordable and environmentally friendly chemical solution deposition technique with great potential for the preparation of complex oxide thin films. In the PAD technique, stable metal–polymer solutions are used as film precursors, and the polymer not only controls the solution viscosity but also binds the metal ions to form a homogeneous solution[26–28]. As a chemical solution route, PAD provides an attractive opportunity to grow films close to thermodynamic equilibrium conditions. The characteristic growth conditions of PAD have already been shown to be advantageous for the stabilization of materials with complex structures or chemical composition, such as misfit cobalt oxides[29] and $Y_3Fe_5O_{12}$ yttrium iron garnet[30]. On the other hand, PAD might also be useful to clarify the role of structural strain in stimulating spontaneous cationic ordering because it has been shown that structural strain accommodation may proceed in a different way in samples prepared by PAD. As demonstrated in epitaxial $La_{0.7}Sr_{0.3}MnO_3$ thin films grown on STO, structural accommodation through complex rotation of the MnO_6 octahedra is different in films grown by PLD and PAD[31].

Since material properties and hence functionality strongly depend on the preparation method and processing steps, in the present work, we report the successful epitaxial growth of highly ordered LCMO double perovskite thin films on (001)-STO substrates by PAD. Epitaxial films with thicknesses in the range of 3–30 nm with excellent magnetic properties ($Msat \approx 6\ \mu_B$/f.u. and $Tc \approx 230$ K) were prepared. Films are in-plane (IP) fully strained with a flat surface displaying root mean squared (RMS) surface roughness values of <1 nm. No signals were detected from secondary phases. A powerful confirmation of the spontaneous B-site cationic ordering was obtained through aberration-corrected scanning transmission electron microscopy (STEM) measurements. Atomically resolved elemental electron energy loss spectroscopy (EELS) maps made evident the ordered occupancy of B–B′ sites by Co–Mn cations, as inferred from the optimal values of the *Msat* and Curie temperature.

materials and methods

Thin film growth

The PAD technique relies on the use of water-soluble polymers with functional $-NH_2$ groups that coordinate cations and prevent their hydrolysis. The polymers used should be compatible with the metal precursors and should undergo clean decomposition upon heating[27]. The

precursor solution for the growth of the LCMO thin film was prepared by mixing three separate aqueous solutions of La, Co, and Mn bound to polymers. Separate solutions were prepared using high-purity (>99.9%) metal salts of lanthanum(III) nitrate, cobalt(II) nitrate, and Mn(II) nitrate. The polymer used in the experiment was branched polyethyleneimine (PEI), average *Mw* ~25,000, and ethylenediaminetetraacetic acid (EDTA) was used as a complexing agent; both were from Sigma Aldrich. Water used in the solution preparation was purified using a Milli-Q water treatment system.

In detail, individual solutions of the different metal ions were prepared by dissolving the corresponding nitrate salts in water and EDTA (1:1 molar ratio). PEI was incorporated into the solution in a 1:1 mass ratio with EDTA. Each individual solution was filtrated using Amicon® filtration units (10 kDa), and retained portions were analyzed by inductively coupled plasma (ICP) (*Optima* 4300™ *DV ICP-OES Perkin-Elmer*). The final concentrations of the solutions used in this work were [La] = 230.4 mM, [Co] = 146.4 mM, and [Mn] = 176.4 mM. The solutions were mixed according to the desired La:Co:Mn 2:1:1 final stoichiometry and concentrated to reach a final cation concentration of ≈61 mM with respect to Mn. These conditions were adjusted to produce films in the range of ≈20–30 nm. Similarly, more diluted solutions were adjusted to obtain films in the range of a few nm (3–5 nm).

The precursor solutions obtained in this way were spin coated on top of 0.5 × 0.5 cm^2 (001)-STO substrates from *Crystec*, GmbH, Germany. Prior to deposition, the as-received substrates were chemically etched and thermally treated to create TiO_2-terminated substrates with atomically flat terraces[32]. After the polymeric layer was deposited, it was annealed in a horizontal tube furnace under an oxygen flow to eliminate the presence of oxygen vacancies. The precursor films were slowly heated from room temperature to 500 °C, and the ramp was stopped for 60 min to ensure that the solvent was evaporated and the polymer decomposed at a slow rate to avoid the formation of pinholes and cracks. PEI decomposes at ≈550 °C, i.e., immediately before the crystallization of the inorganic film. The metal ions are released to form oxides after polymer decomposition, and higher substrate temperatures will lead to the growth of epitaxial films[27,28]. Therefore, after the step, the samples were heated at a ramp rate of 3 °C/min from 800 °C to 950 °C for film crystallization. The cooling ramp was also set at 3 °C/min.

Characterization of the structural and physical properties

The structural properties of the epitaxial films were studied by X-ray diffraction and reflectivity using a D5000 (Siemens) diffractometer, an X'Pert MRD (PANalytical) four-angle diffractometer with monochromatic Cu-Kα1 radiation (1.54060 Å) and a Bruker D8 Advance GADDS system. Magnetization measurements were performed using a superconducting quantum interference device (SQUID; Quantum Design) as a function of temperature and magnetic field. External magnetic fields were applied both parallel (IP configuration) and perpendicular (OP configuration) to the sample plane. The diamagnetic contribution of the substrate and other instrumental contributions were properly corrected[33]. The relative error in the determination of the *Msat* was ~5% and was mostly attributable to the error in the estimation of the film volume. The surface topography of the films was investigated by atomic force microscopy (AFM) using an Asylum Research MFP-3D microscope in tapping mode. The microstructure of the LCMO film and the B-site ordering at the atomic scale were studied using STEM in combination with EELS. Specimens for STEM were prepared by conventional methods, grinding, and Ar-ion milling. The STEM images and EELS spectral images were acquired with an aberration-corrected Nion UltraSTEM™ 200 operated at 200 kV and equipped with a 5th order Nion aberration corrector. The particular geometry of these microscopes allows for the simultaneous acquisition of different signals from two singular detectors.

Results and discussion

After a careful optimization process (see Supporting Information), we determined the ideal growth conditions (growth temperature of 900 °C, annealing time of ~1 h, and oxygen flow above 0.3 l/min) to obtain the optimal magnetic properties, which were close to the theoretically expected values. Samples prepared under other conditions show depressed magnetization values.

A typical XRD pattern corresponding to an LCMO film annealed at 900 °C on an STO substrate is shown in Fig. 1. The corresponding film thickness, extracted from the X-ray reflectivity measurements, is ~10 nm (Supporting Information, Fig. S1). The epitaxial nature of the LCMO film is evidenced by the detection of only (001) peaks along with the corresponding STO-(001) peaks originating from the STO-(001) substrate and the K_β reflection (see Fig. 1a). An out-of-plane lattice parameter c = 3.859 Å is estimated from the high-resolution X-ray diffraction pattern of the (002) diffraction peak (see Fig. 1b).

The film is IP fully strained with a lattice mismatch of ~0.4%. The 3D reciprocal space tomography reveals the presence of superstructure peaks of the type $(\boldsymbol{hk}\frac{\boldsymbol{l}}{2})$ (l = odd), and the absence of reflections of the type $(\frac{\boldsymbol{h}}{2}\boldsymbol{kl})$ (h = odd) and $(\boldsymbol{h}\frac{\boldsymbol{k}}{2}\boldsymbol{l})$ (k = odd) indicates that the cell of LCMO ($\sqrt{2}a_p \times \sqrt{2}a_p \times 2a_p$, with a_p = primitive perovskite) is oriented with the c-direction out of plane (OP) (Supporting Information, Fig. S2). The epitaxial nature of the LCMO films is further confirmed by the reciprocal space maps around the STO-(103) reflection that reveal that the

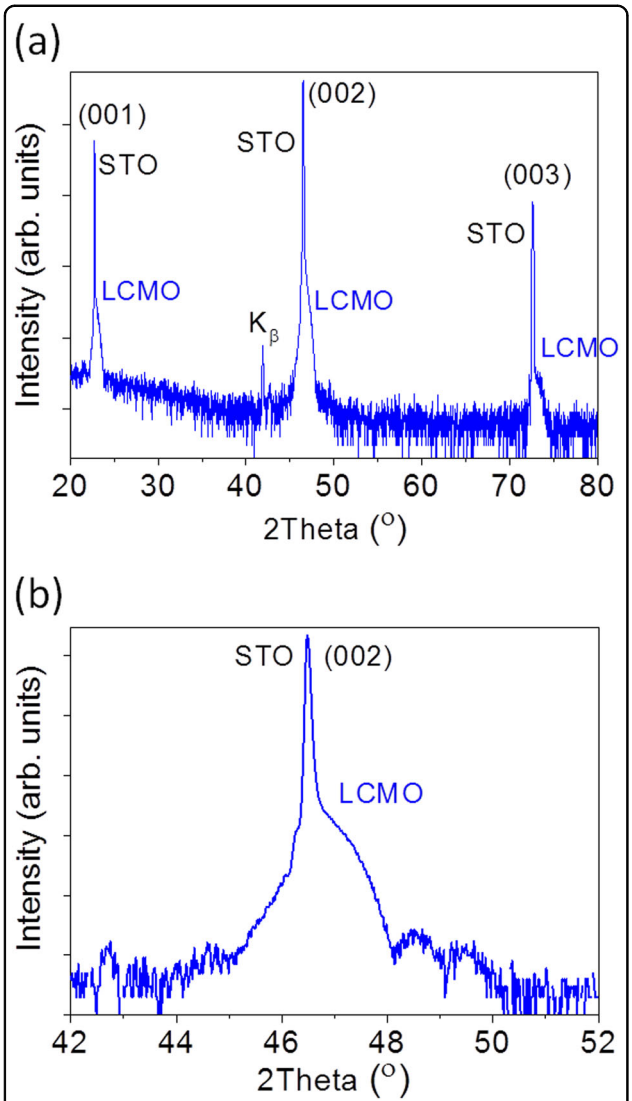

Fig. 1 a X-ray diffraction pattern of 10 nm thick LCMO/STO film grown at 900 °C. The (001) peaks of the LCMO film and STO substrate are indicated. **b** High-resolution XRD pattern of the (002) diffraction peak. The oscillations around the main diffraction peak are an indication of the high structural quality of the epitaxial LCMO films

films grow epitaxially, cube-on-cube and fully strained with the STO substrate (Supporting Information, Fig. S3).

In addition, the AFM topography images displayed in Fig. 2 show flat surfaces with an RMS surface roughness value of <1 nm, thus indicating that the samples have a high microstructural quality. Fig. 2a, b clearly shows the terrace-like morphology imposed by the conformal growth on top of the substrate steps.

The magnetic properties of a 26-nm-thick LCMO/STO thin film grown at 900 °C for 60 min with an oxygen flow of 0.3 l/min are shown in Fig. 3. Figure 3a shows the temperature dependence of magnetization (zero field cooling and field cooling measurements) in the temperature range from 10 K to 300 K under a magnetic field of $H = 1$ kOe applied along the IP direction. The Curie temperature $Tc = 230$ K was estimated from the minimum of the function *(1/M)(dM/dT)*. No signals for the coexistence of different FM phases, as usually occurs in oxygen-deficient samples prepared by PLD or sputtering[10,23], are detected; thus, we assume that the samples are fully oxygenated. In Fig. 3b, the measured low temperature (10 K) $Msat \approx 5.9\ \mu_B$/f.u. and IP coercive field of $Hc \approx 10$ kOe agree well with the data reported for B-site ordered LCMO bulk[34] and thin film samples[20,23,25]. On the other hand, samples not grown under optimal conditions show depressed magnetization values (Supporting Information, Fig. S4). Even though the XRD data cannot provide information regarding B-site cationic ordering, in addition to the improvement in the magnetic properties, the degree of crystallinity and the microstructural film quality also improve with increasing annealing time and oxygen flux, as shown in the reciprocal space maps displayed in Fig. S3 in the Supporting Information.

The high values of *Msat* and *Tc* indicate a high degree of Co/Mn cationic ordering. As mentioned previously, both values are very sensitive to cationic ordering and are substantially reduced in disordered samples. As indicated above, FM ordering in the insulating LCMO originates from the superexchange interaction between Co^{2+} ions in the high spin state ($3d^7$: $t_{2g}^5\ e_g^2$) with half-filled e_g orbitals and the overall spin $S = 3/2$ and Mn^{4+} ions ($3d^3$: $t_{2g}^3\ e_g^0$) with empty e_g orbitals and $S = 3/2$ mediated by oxygen anions, according to the Goodenough–Kanamori–Anderson rules[14–16]. As a result, a large theoretical saturation spin only moment, $Msat = 6\ \mu_B$/f.u. and a relatively high value of T_C ~230 K are predicted. In this scenario, cationic disorder promotes the appearance of Mn^{4+}–O–Mn^{4+} and Co^{2+}–O–Co^{2+} bonding, generating antiferromagnetic superexchange interactions and lowering both the *Msat* and the Curie temperature in partially disordered samples.

Figure 3b also shows the strong anisotropic behavior of the samples. When the magnetic field is applied perpendicular to the sample plane (the OP configuration), saturation is reached at ~30 kOe, while when the field is applied parallel to the sample plane (the IP configuration), saturation is not reached even at 80 kOe. Thus, the perpendicular-to-plane direction is the easy magnetization direction, as previously observed in samples grown by RF magnetron sputtering[23,35]. Our previous results for samples prepared by RF sputtering indicate that the Co^{2+} valence state is preferentially stabilized irrespective of the structural strain even in nonstoichiometric samples[36]. In addition, it was also shown that anisotropy in LCMO films is mainly driven by spin-orbit coupling of Co^{2+} and is strain-dependent. Under tensile strain, as in LCMO films grown on STO, a strong increase in the angular

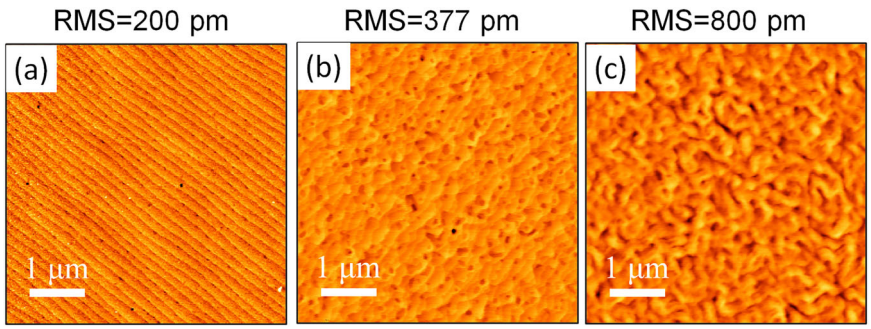

Fig. 2 AFM surface topography images ($5 \times 5\ \mu m^2$) of samples with different thicknesses, **a** 3 nm, **b** 10 nm, and **c** 26 nm, grown at 900 °C for 30 min with an oxygen flow of 0.3 l/min showing RMS roughness values well below 1 nm; **a** and **b** clearly show the terrace-like morphology imposed by the conformal growth on top of the substrate steps

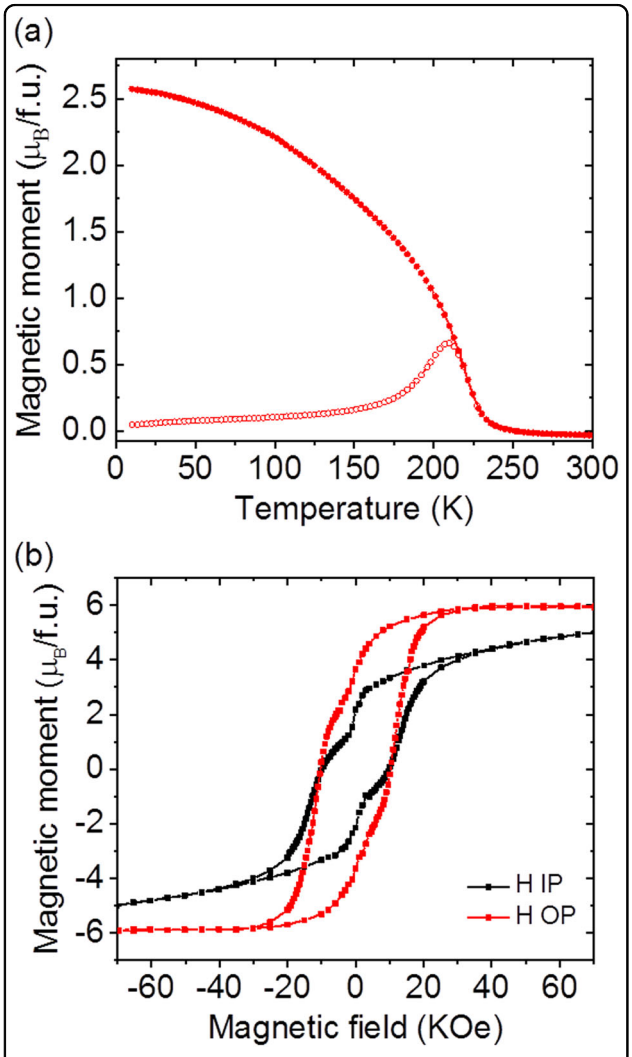

Fig. 3 a Magnetization vs temperature of an LCMO/STO film of 26 nm grown at 900 °C measured after zero field cooling (open symbols) and field cooling (solid symbols) with a magnetic field of 1 KOe in-plane. **b** M–H loops recorded at 10 K by applying a mmradagnetic field parallel to (100)-STO, in-plane; and parallel to (001)-STO, out of plane

contribution to the magnetic moment of Co^{2+} occurs and generates a strong perpendicular magnetic anisotropy[35,36], as in the present case. On the other hand, *M(H)* loops in Fig. 3b show the typical bi-loop shape recurrent in many cases reported in the literature[10,22]. The origin of this sudden drop in the remanent magnetization at $H = 0$, which has been erroneously attributed in some cases to the existence of two magnetic domains possessing different coercivities[10], is due to the existence of antiphase boundaries. Antiphase boundaries appear because the nucleation of Co^{2+} and Mn^{4+} cationic ordering may occur at different positions in different regions of the sample, and when regions with inverted Co^{2+} and Mn^{4+} positions relative to the other merge together, an antiphase boundary is formed. As noted by Dass and Goodenough[8], at the antiphase interface of Co^{2+}–O–Co^{2+} or Mn^{4+}–O–Mn^{4+}, AF interactions occur; thus, lowering the field from saturation at $H = 0$ causes any antiphase regions to revert back to an antiparallel orientation with a 180° change in the spin orientation across an antiphase boundary, which would produce the observed sudden drop in the remnant magnetization. This drop is more pronounced in thinner films (Supporting Information, Fig. S5), indicating a larger contribution of antiphase boundaries on the magnetic hysteresis loops. Accordingly, the bi-loop features of the hysteresis cycle are not observed in samples without extended antiphase boundaries or with ordered regions separated by a blurred disordered boundary region[25]. Therefore, from the magnetic measurements, we conclude that our LCMO films present almost full Mn^{4+}–Co^{2+} cationic ordering.

Aberration-corrected STEM images obtained for optimally grown films give further support to the high B-site cationic ordering degree of films grown by the PAD approach. As mentioned above, the particular geometry of the microscope used allows for acquiring different signals simultaneously from two singular detectors in such a way that electrons that are scattered at high angles are

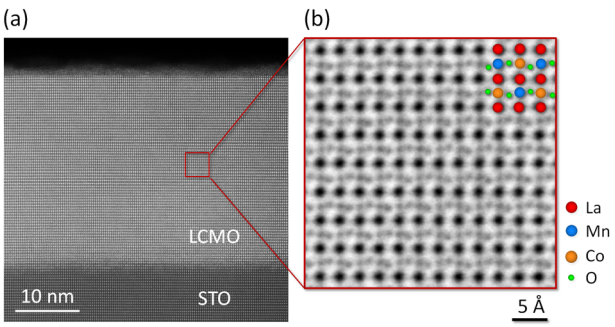

Fig. 4 a *Z*-contrast image of an optimally grown LCMO/STO film. **b** ABF image of the LCMO structure. The probe-forming aperture half angle was 30 mrad, and the half angles of the ABF detector spanned from 15 to 30 mrad. Both images are viewed along the [110] pseudocubic projection, which allows visualization of the buckling of the O sublattice. Inset in **b**, schematics of the LCMO structure showing the distortions revealed by the ABF image

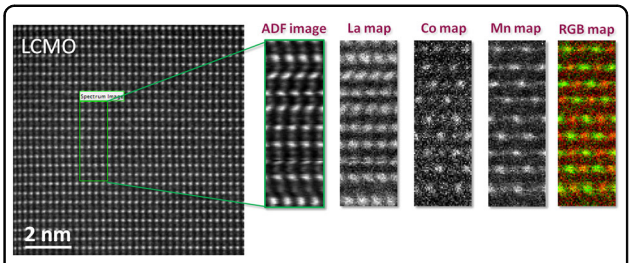

Fig. 5 From left to right, *Z*-contrast image of the LCMO film, ADF image, atomic maps of the La M, Co L, and Mn L absorption edges and the RGB map produced by overlaying the Co (in red) and Mn (in green) elemental maps. The inset in the *Z*-contrast image shows the region where a spectral image was acquired. The spectral image was acquired along the [110]-zone axis for visualizing the B-site ordering

recorded with a high angle annular detector that produces a contrast interpretable in terms of the atomic number *Z* of the different atomic species. Thus, this is an effective structure imaging mode specifically for the atomic scale[37]. Simultaneously, those electrons that are scattered at much lower angles can be collected by an annular bright field (ABF) detector, which is a direct beam disk that allows the imaging of light and heavy atoms in a single STEM image, thus probing the *A*, *B*, and *O* sublattices of the ABO_3-perovskite structure[38,39]. The coherent interference of such electrons results in a phase image that presents an inverted contrast with respect to the *Z*-contrast images. Fig. 4a, b show a *Z*-contrast image of the 30-nm-thick LCMO film and a higher magnification ABF image of the LCMO structure. Both images were acquired along the [110] pseudocubic projection, which allows visualization of the BO_6 octahedral rotation and the buckling of the *O* sublattice of LCMO, as clearly seen in Fig. 4b. Such rippling is due to the presence of octahedral tilts along the $[100]_{pc}$ and $[010]_{pc}$ directions[8,34]. The structure and chemistry of the material can be probed simultaneously by using another imaging detector, such as an electron energy loss spectrometer, together with the high angle annular detector.

Figure 5 shows from left to right the *Z*-contrast image of the LCMO structure from which the spectrum image (see marked area in green) was acquired, the simultaneously acquired annular dark field (ADF) image, the atomic resolution maps of the La M, Co L, and Mn L absorption edges and the RGB image produced by overlaying the Co (in red) and Mn (in green) elemental maps. Whereas the La elemental map shows a continuous A-site contrast, both Co and Mn maps show an intensity variation in every other B-site atomic column, consistent with ordering. Indeed, the checkerboard pattern evidenced by the RGB map unambiguously demonstrates the Co/Mn ordering of the LCMO phase. Therefore, STEM images provide powerful confirmation that PAD growth promotes the desired double perovskite cationic ordering, as inferred from the optimal values of the *Msat* and Curie temperature.

To date, there is no clear knowledge regarding the mechanism controlling B-site cationic ordering, and efforts to attain it have been mainly focused on obtaining two well-differentiated B-sites so that different cations will spontaneously choose one of them according to steric or charge distribution criteria. In this regard, it was recently claimed that a high degree of cationic ordering can be obtained by growing LCMO on (111)-STO substrates instead of the commonly used (001)-STO[22].

It was argued that (111)-substrate growth induces an "in-plane" strain that combined with the intrinsically tilted oxygen octahedra, following the $a^-a^-c^+$ scheme of the $P2_1/n$ (monoclinic) space group[40], generates the formation of two different sized B-site spaces in a rock salt arrangement. This particular arrangement would promote the desired double perovskite cationic ordering, resulting in excellent magnetic properties. However, authors in ref. [22] report fully strained epitaxial growth on the (111) substrate incompatible with the monoclinic crystal system but compatible with the trigonal one. It is worth mentioning that many single perovskites crystallize in the rhombohedral $R\bar{3}c$ space group (e.g., $LaCoO_3$[41], $LaNiO_3$[42], and $La_{2/3}Sr_{1/3}MnO_3$[43]). Thus, this crystal system can naturally accommodate the strain imposed by the (111) orientation of the substrate with the $a^-a^-a^-$ octahedral tilting scheme without creating two differently sized B-site cages. In addition, it is important to remark that the conclusion regarding the higher degree of cationic ordering in samples prepared on (111)-STO substrates was derived by comparing magnetization values measured with the magnetic field applied parallel to the sample plane and that, in the case of the (001)-STO samples, corresponds to the hard magnetization direction.

Therefore, the lower values of the magnetization obtained in the (001)-STO samples do not necessarily imply a lower cationic ordering but result from the strong perpendicular magnetic anisotropy present in the (001)-oriented LCMO thin films[35].

It has also been proposed that growth instabilities at the growth front may be a possible alternative to induce spontaneous B-site cationic ordering. The notable differences between thermal evaporation methods and CSD techniques represent clearly different approaches. Undoubtedly, in CSD techniques, the microstructure and orientation of the thin films can be significantly influenced by the solution and material chemistry, substrate characteristics, and annealing conditions. Moreover, in the PAD method, the direct binding between the metal and polymer stabilizes the metal complexes so that they do not experience preformation in the solution prior to polymer decomposition[44], thus increasing the lifetime of the solution and preventing early metal oxide formation during the deposition stage. Thermogravimetric analysis indicated complete degradation of the polymer above ≈550 °C, and the high thermal stability of PEI prevents the formation of the oxide film phase below this temperature. Consequently, the removal of the organic material and the crystallization of the film both take place at the same temperature[27,28]. Furthermore, the slow decomposition of the polymer promotes the formation of the inorganic film at a very slow rate close to thermodynamic equilibrium conditions and promotes its high crystallinity and quality. Thus, the nucleation and growth processes in PAD films are substantially different from those occurring in films prepared by thermal evaporation. In the latter case, atomic species arrive at the substrate surface, typically at a temperature close to 900 °C, with kinetic energies in the range from tens of eV to a few hundred eV, and they have to thermalize. Therefore, crystallization and film growth occur far from thermodynamic equilibrium conditions[45]; i.e., surface diffusion is high and atomic species can move easily, which might make B-site cationic ordering difficult and require the use of ulterior high temperature annealing processes to improve it. In contrast, the formation and crystallization of a solid phase from liquid-based solutions requires a much smaller thermodynamic-driving force than thermal evaporation methods[18]. Thus, in films prepared by PAD, crystallization of the oxide takes place near the decomposition temperature of the polymer, i.e., 550 °C, i.e., close to thermodynamic equilibrium conditions. The slow growth conditions of PAD can be much more favorable for attaining spontaneous B-site cationic ordering, as observed in our case. In fact, PAD has been revealed as a very appropriate method to prepare complex oxide phases with complex cationic ordering[28].

Conclusions

High-quality epitaxial LCMO films have been prepared with a single one-step growth process using the PAD technique on top of STO (001)-oriented substrates. The magnetic properties of the films ($Msat \approx 6\ \mu_B$/f.u. and $Tc \approx 230$ K) are indicative of almost full Co/Mn B-site cationic ordering. Further support for the existence of full Co/Mn cationic ordering is obtained by STEM measurements; EELS maps indicate the ordered occupancy of B–B′ sites by Co/Mn cations. The magnetic properties of LCMO are highly sensitive to B-site cationic ordering; therefore, obtaining full cationic ordering is fundamental for potential technological applications. To date, there is no clear knowledge regarding the mechanism controlling B-site cationic ordering, and different strategies relying on structural strain and growth instabilities have been proposed but without conclusive results. In this work, we show that the particular crystallization and growth process conditions of PAD (very slow rate, close to thermodynamic equilibrium conditions) promote the high crystallinity and quality of the films, as well as B-site cationic ordering. We believe that the obtained results show the advantage of the CSD–PAD method over physical methods (far from thermodynamic equilibrium growth) to optimize B-site ordering as well as the desirable physical properties of functional double perovskite oxide thin films. In addition, in the context where the demand for sustainable and environmentally friendly reactants and processes steadily increases, PAD is based in aqueous solutions of environmentally friendly metal salts and commercially available polymers.

Acknowledgements

We acknowledge financial support from the Spanish Ministry of Economy and Competitiveness through the Severo Ochoa Programme for Centres of Excellence in R&D (SEV-2015-0496), COACHSUPENERGY project (MAT2014-51778-C2-1-R) and MAT2015-71664-R, cofinanced by the European Regional Development Fund. Support from the European Union's Horizon 2020 Research and Innovation Programme under the Marie Sklodowska-Curie grant agreement no. 645658 (DAFNEOX Project) is also acknowledged. H.W. acknowledges financial support from the China Scholarship Council (CSC). J.G. also acknowledges the Ramon y Cajal program (RYC-2012-11709). The STEM–EELS analysis was sponsored by the U.S. Department of Energy, Office of Science, Basic Energy Sciences, Materials Sciences and Engineering Division. The authors would like to thank Anna Crespi and Francesc Xavier Campos for assistance with the 3D reciprocal space tomography and reciprocal space map measurements.

Conflict of interest

The authors declare no conflict of interest.

Supplementary information is available for this paper at https://doi.org/10.1038/s41427-019-0144-8.

Received: 13 February 2019 Revised: 2 May 2019 Accepted: 18 May 2019
Published online: 02 August 2019

References

1. Tokura, Y. & Hwang, H. Y. Condensed-matter physics: complex oxides on fire. *Nat. Mater.* **7**, 694–695 (2008).
2. Rondinelli, J. M. & Spaldin, N. A. Structure and properties of functional oxide thin films: insights from electronic-structure calculations. *Adv. Mater.* **23**, 3363–3381 (2011).
3. Martin, L. W., Chu, Y. H. & Ramesh, R. Advances in the growth and characterization of magnetic, ferroelectric, and multiferroic oxide thin films. *Mater. Sci. Eng. R. Rep.* **68**, 89–133 (2010).
4. Ohtomo, A. & Hwang, H. Y. A high-mobility electron gas at the $LaAlO_3/SrTiO_3$ heterointerface. *Nature.* **427**, 423–426 (2004).
5. Moritomo, Y. et al. Electronic structure of double-perovskite transition-metal oxides. *Phys. Rev. B.* **61**, R7827–R7830 (2000).
6. Hua, B. et al. The excellence of both worlds: developing effective double perovskite oxide catalyst of oxygen reduction reaction for room and elevated temperature applications. *Adv. Funct. Mater.* **26**, 4106–4112 (2016).
7. Vasala, S. & Karppinen, M. $A_2B'B''O_6$ perovskites: a review. *Prog. Solid State Chem.* **43**, 1–36 (2015).
8. Dass, R. I. & Goodenough, J. B. Multiple magnetic phases of $La_2CoMnO_{6-\delta}(0 < \sim\delta < \sim0.05)$. *Phys. Rev. B.* **67**, 014401 (2003).
9. Kyômen, T., Yamazaki, R. & Itoh, M. Correlation between Magnetic Properties and Mn/Co Atomic Order in $LaMn_{0.5}Co_{0.5}O_{3+\delta}$: I. Second-Order Nature in Mn/Co Atomic Ordering and Valence State. *Chem. Mater.* **15**, 4798–4803 (2003).
10. Guo, H. Z., Gupta, A., Zhang, J., Varela, M. & Pennycook, S. J. Effect of oxygen concentration on the magnetic properties of La_2CoMnO_6 thin films. *Appl. Phys. Lett.* **91**, 202509 (2007).
11. Truong, K. D., Laverdière, J., Singh, M. P., Jandl, S. & Fournier, P. Impact of Co/Mn cation ordering on phonon anomalies in La_2CoMnO_6 double perovskites: Raman spectroscopy. *Phys. Rev. B.* **76**, 132413 (2007).
12. Mao, Y. Facile molten-salt synthesis of double perovskite La_2BMnO_6 nanoparticles. *RSC Adv.* **2**, 12675–12678 (2012).
13. López-Mir, L. et al. Anisotropic sensor and memory device with a ferromagnetic tunnel barrier as the only magnetic element. *Sci. Rep.* **8**, 861 (2018).
14. Goodenough, J. B. An interpretation of the magnetic properties of the perovskite-type mixed crystals $La_{1-x}Sr_xCoO_{3-\lambda}$. *J. Phys. Chem. Solids.* **6**, 287–297 (1958).
15. Kanamori, J. Superexchange interaction and symmetry properties of electron orbitals. *J. Phys. Chem. Solids.* **10**, 87–98 (1959).
16. Anderson, P. W. Antiferromagnetism. Theory of superexchange interaction. *Phys. Rev.* **79**, 350–356 (1950).
17. Goodenough, J. B., Wold, A., Arnott, R. J. & Menyuk, N. Relationship between crystal symmetry and magnetic properties of ionic compounds containing Mn^{3+}. *Phys. Rev.* **124**, 373–384 (1961).
18. Koster, G., Huijben, M. & Rijnders, G. Chemical solution deposition techniques for epitaxial growth of complex oxides. in *Epitaxial Growth of Complex Metal Oxides*, Ch. 4 (Woodhead Publishing, Cambridge, UK, 2015) 69–93.
19. Schneller, T., Waser, R., Kosec, M. & Payne, D. *Chemical Solution Deposition of Functional Oxide Thin Films*. (Springer-Verlag, Wien, 2013) 1–796.
20. Guo, H. Z., Gupta, A., Calvarese, T. G. & Subramanian, M. A. Structural and magnetic properties of epitaxial thin films of the ordered double perovskite La_2CoMnO_6. *Appl. Phys. Lett.* **89**, 262503 (2006).
21. Singh, M. P., Charpentier, S., Truong, K. D. & Fournier, P. Evidence of bidomain structure in double-perovskite La_2CoMnO_6 thin films. *Appl. Phys. Lett.* **90**, 211915 (2007).
22. Kleibeuker, J. E. et al. Route to achieving perfect B-site ordering in double perovskite thin films. *NPG Asia Mater.* **9**, e406 (2017).
23. Galceran, R. et al. Engineering the microstructure and magnetism of $La_2CoMnO_{6-\delta}$ thin films by tailoring oxygen stoichiometry. *Appl. Phys. Lett.* **105**, 242401 (2014).
24. Chakraverty, S., Yu, X. Z., Kawasaki, M., Tokura, Y. & Hwang, H. Y. Spontaneous B-site order and metallic ferrimagnetism in $LaSrVMoO_6$ grown by pulsed laser deposition. *Appl. Phys. Lett.* **102**, 222406 (2013).
25. Egoavil, R. et al. Phase problem in the B-site ordering of La_2CoMnO_6: impact on structure and magnetism. *Nanoscale.* **7**, 9835–9843 (2015).
26. Jia, Q. X. et al. Polymer-assisted deposition of metal-oxide films. *Nat. Mater.* **3**, 529–532 (2004).
27. Zou, G. F. et al. Polymer-assisted-deposition: a chemical solution route for a wide range of materials. *Chem. Soc. Rev.* **42**, 439–449 (2013).
28. Vila-Fungueiriño, J. M. et al. Polymer assisted deposition of epitaxial oxide thin films. *J. Mater. Chem. C.* **6**, 3834–3844 (2018).
29. Rivas-Murias, B., Vila-Fungueirino, J. M. & Rivadulla, F. High quality thin films of thermoelectric misfit cobalt oxides prepared by a chemical solution method. *Sci. Rep.* **5**, 11889 (2015).
30. Lucas, I. et al. Chemical solution synthesis and ferromagnetic resonance of epitaxial thin films of yttrium iron garnet. *Phys. Rev. Mater.* **1**, 074407 (2017).
31. Vila-Fungueiriño, J. M. et al. Thermodynamic conditions during growth determine the magnetic anisotropy in epitaxial thin-films of $La_{0.7}Sr_{0.3}MnO_3$. *J. Phys. D.* **49**, 315001 (2016).
32. Kareev, M. et al. Atomic control and characterization of surface defect states of TiO_2 terminated $SrTiO_3$ single crystals. *Appl. Phys. Lett.* **93**, 061909 (2008).
33. Stamenov, P. & Coey, J. M. D. Sample size, position, and structure effects on magnetization measurements using second-order gradiometer pickup coils. *Rev. Sci. Instrum.* **77**, 015106 (2006).
34. Baron-Gonzalez, A. J., Frontera, C., Garcia-Munoz, J. L., Rivas-Murias, B. & Blasco, J. Effect of cation disorder on structural, magnetic and dielectric properties of La_2MnCoO_6 double perovskite. *J. Phys. Condens. Matter.* **23**, 496003 (2011).
35. Galceran, R. et al. Strain-induced perpendicular magnetic anisotropy in $La_2CoMnO_{6-\epsilon}$ thin films and its dependence on film thickness. *Phys. Rev. B.* **93**, 144417 (2016).
36. López-Mir, L. et al. Magnetic anisotropy and valence states in $La_2Co_{1-x}Mn_{1+x}O_6$ ($x \approx 0.23$) thin films studied by x-ray absorption spectroscopy techniques. *Phys. Rev. B.* **95**, 224434 (2017).
37. Nellist, P. D. & Pennycook, S. J. Incoherent imaging using dynamically scattered coherent electrons. *Ultramicroscopy.* **78**, 111–124 (1999).
38. Okunishi, E. et al. Visualization of light elements at ultrahigh resolution by STEM annular bright field microscopy. *Microsc. Microanal.* **15**(S2), 164–165 (2009).
39. Ishikawa, R. et al. Direct imaging of hydrogen-atom columns in a crystal by annular bright-field electron microscopy. *Nat. Mater.* **10**, 278–281 (2011).
40. Woodward, P. M. Octahedral tilting in perovskites. I. geometrical considerations. *Acta Crystallogr. Sect. B Struct. Sci.* **53**, 32–43 (1997).
41. Thornton, G., Tofield, B. C. & Hewat, A. W. A neutron diffraction study of $LaCoO_3$ in the temperature range $4.2 < T < 1248$ K. *J. Solid State Chem.* **61**, 301–307 (1986).
42. García-Muñoz, J. L., Rodríguez-Carvajal, J., Lacorre, P. & Torrance, J. B. Neutron-diffraction study of $RNiO_3$(R = La,Pr,Nd,Sm): electronically induced structural changes across the metal-insulator transition. *Phys. Rev. B.* **46**, 4414–4425 (1992).
43. Radaelli, P. G. et al. Structural effects on the magnetic and transport properties of perovskite $A_{1-x}A_x'MnO_3$($x = 0.25, 0.30$). *Phys. Rev. B.* **56**, 8265–8276 (1997).
44. Burrell, A. K., Mark McCleskey, T. & Jia, Q. X. Polymer assisted deposition. *Chem. Commun.* **11**, 1271–1277 (2008).
45. Greene, J. E. Thin film nucleation, growth, and microstructural evolution: an atomic scale view. in *Handbook of Deposition Technologies for Films and Coatings* 3rd edn (ed. Martin, P. M.) Ch. 12 (William Andrew Publishing, Boston, 2010) 554–620.